Cleveland State University
EngagedScholarship@CSU

Mechanical Engineering Faculty Publications | Mechanical Engineering Department

1997

Diophantine Type Fractional Derivative Representation of Structural Hysteresis, Part II: Fitting, Computational Mechanics

Jerzy T. Sawicki
Cleveland State University, j.sawicki@csuohio.edu

Joe Padovan
University of Akron

Follow this and additional works at: https://engagedscholarship.csuohio.edu/enme_facpub

 Part of the Mechanical Engineering Commons

How does access to this work benefit you? Let us know!

Original Citation

Sawicki, J.T., and Padovan, J. (1997). Diophantine Type Fractional Derivative Representation of Structural Hysteresis, Part II: Fitting. Computational Mechanics, 19(5), 341-356, doi: 10.1007/s004660050183.

This Article is brought to you for free and open access by the Mechanical Engineering Department at EngagedScholarship@CSU. It has been accepted for inclusion in Mechanical Engineering Faculty Publications by an authorized administrator of EngagedScholarship@CSU. For more information, please contact library.es@csuohio.edu.

Diophantine type fractional derivative representation of structural hysteresis

Part II: Fitting

J. T. Sawicki, J. Padovan

Abstract Part I of this series introduced the diophantinized fractional model and the decompositional formulation. The various important properties of fractional continuum formulation and its decomposed version were developed. In Part II the dynamic properties of the diophantine representation are investigated. The model fitting scheme will be developed to handle an arbitrary frequency dependent structural hysteriesis. This is followed up with the results of benchmark studies which demonstrate the effectiveness of fitting.

1 Introduction

To make a more workable fractional differintegro representation of structural hysteresis, a diophantine, Schmidt (1980), type formulation was introduced in Part I of this series of papers, Padovan and Sawicki (1996). This included both the composed and decomposed versions. Because of the operator properties, the decomposed formulation can be cast in either a scalar or vector format. The paper also explored the various solution properties and asymptotic characteristics.

In this part, the primary focus will be to introduce a fitting scheme along with a investigation of the eigen properties. The primary thrust of the fitting procedure will be to enable the handling of arbitrary frequency dependent force deflection behavior. This of course is done within the linear context. In this way frequency dependent hysteresis can be represented. The vector form of the decomposed version of the diophantine simulation yields a more workable formulation.

In the sections which follow detailed discussions are given on

1) The dynamic properties of the diophantine representation
2) Modelling via a remezed, see Remez (1934), Carpenter and Varga (1991), Hamming (1962) least square scheme, Hamming (1962), and
3) An evaluation of the modelling performance.

Note, the evaluation phase will investigate the eigen properties, phasing and amplitude response as a function of diophantine fractional order. The generality of the overall procedure is such that both transient and steady response can be handled.

J. T. Sawicki
Department of Mechanical Engineering,
Cleveland State University, Cleveland, Ohio 44115, USA

J. Padovan
Departments of Mechanical and Polymer Engineering,
The University of Akron, Akron, Ohio 44325-3903, USA

Correspondence to: J. Padovan

2 Dynamic properties of diophantine representation

In Part I, two major issues were considered, i.e., 1) the introduction of the diophantinized fractional model, and 2) the decompositional formulation. As was seen, under the use of diophantine approximations, both the fractional continuum formulation and its decomposed version have the same poles – eigenvalues. These can be established via the use of the Laplace transform. To determine the long time steady state – amplitude frequency and phase shift behavior, the Fourier transform, i.e., harmonic response can be sought. Such issues will be addressed in the following subsections.

2.1 General MKV formulation

For the general MKV formulation, the governing equations are, Padovan and Sawicki (1996),

$$M\ddot{x} + F_D + Kx = S(t) \tag{2.1}$$

$$\sum_{\ell=0}^{N_f} \mu_{f\ell} D_{a_\ell}(F_D) = \sum_{\ell=1}^{N_x} \mu_{x\ell} D_{b_\ell}(x) \tag{2.2}$$

Taking the Laplace transform of (2.1 and 2) yields

$$\left(s^2 M + K\right) X_S + F_{DS} = S_S \tag{2.3}$$

$$\left(\sum_{\ell=0}^{N_f} \mu_{f\ell}(s)^{a_\ell}\right) F_{DS} = \left(\sum_{\ell=0}^{N_x} \mu_{x\ell}(s)^{b_\ell}\right) X_S \tag{2.4}$$

Replacing F_{DS} in (2.4) with (2.3) one obtains

$$\left\{\sum_{\ell}^{N_f}\left((s)^{a_\ell+2} M\mu_{f\ell} + (s)^{a_\ell} K\mu_{f\ell}\right) + \sum_{\ell}^{N_f}(s)^{b_\ell}\mu_{x\ell}\right\} X_S = \sum_{\ell}^{N_x}(s)^{a_\ell}\mu_{f\ell} S_S \tag{2.5}$$

The eigenvalue problem emerges from the homogeneous version of (2.5). Since $X_S \neq 0$, then it follows that

$$\sum_{\ell}^{N_f} (s)^{a_\ell+2} M_{f\ell} + (s)^{a_\ell} K_{f\ell} + \sum_{\ell}^{N_x} (s)^{b_\ell} {}_{x\ell} = 0 \tag{2.6}$$

Contingent on the power sets $a_\ell;\ \ell \in [1, N_f]$ and $b_\ell;\ \ell \in [1, N_x]$, the latent roots-poles of (2.6) form the system eigenvalues. This relation applies for both general fractional exponents as well as their diophantine counterpart. The same is true for the decomposed set.

When a_ℓ and b_ℓ are general fractions, it is somewhat difficult to extract the latent roots of (2.6). Several options can simplify this task, namely

1) a_ℓ and b_ℓ are integer multiples of some fraction, i.e.,

$$a_\ell = \ell / f_a \tag{2.7}$$

$$b_\ell = \ell / f_b \tag{2.8}$$

where f_a and f_b are arbitrary fractions wherein ℓ defines the span

$$\begin{matrix} 1/f_a, 2/f_a, \ldots, N_f/f_a \\ 1/f_b, 2/f_b, \ldots, N_f/f_b \end{matrix} \tag{2.9}$$

or,

2) a_ℓ and b_ℓ are diophantine approximated sets.

If $f_a = f_b$, then by letting

$$(s)^{1/f_a} = \gamma \ , \tag{2.10}$$

(2.6) reduces to the mixed integer relation

$$\sum_{\ell}^{N_f} (\gamma)^{\ell+2f_a} M_{f\ell} + (\gamma)^{\ell} K_{f\ell} + \sum_{\ell}^{N_x} (\gamma)^{\ell} {}_{x\ell} = 0 \tag{2.11}$$

When f_a is itself an integer, then (2.11) reduces to a completely fractable diophantine. Which form is the best depends on the fitting process.

2.2
Decomposed vector form

For the diophantine representation recalling the compositional rule, Padovan and Sawicki (1996), the dynamics and constitutive relations can be recast in the following decomposed vector form

$$D_{\frac{1}{N_x}}(\underline{Y}) = [\Theta]\underline{Y} + \underline{R} \tag{2.12}$$

By applying the Laplace transform to its homogeneous form, the following problem is obtained

$$\left[(s)^{1/N_x}[I] - [\Theta]\right]\underline{Y}(s) = \underline{0} \tag{2.13}$$

By letting

$$\lambda = (s)^{1/N_x} \tag{2.14}$$

(2.13) reduces to the expression

$$[\lambda[I] - [\Theta]]\underline{Y}(s) = \underline{0} \tag{2.15}$$

Here, we have the usual linear eigenvalue problem. Of course, $[\Theta]$ reflects the diophantine representation and the successive applications of the composition rule.

Based on the vector form, adjoint operators can be introduced to establish biorthogonality conditions for eigenvectors of (2.13). In this context we let

$$D_{\frac{1}{N_x}}(\underline{Z}) = [\Theta]^T \underline{Z} \tag{2.16}$$

The eigen problem associated with (2.16) is given by the expression

$$\left[(s)^{1/N_x}[I] - [\Theta]^T\right]\underline{Z}(s) = \underline{0} \tag{2.17}$$

or, due to (2.14), by

$$\left[\lambda[I] - [\Theta]^T\right]\underline{Z}(s) = \underline{0} \tag{2.18}$$

where here, the roots $\underline{\lambda}$ appearing in (2.15 and 18) are the same. Given unique eigenvalues (λ_i, λ_k), then it follows that their associated vectors satisfy the biorthogonality conditions, i.e.,

$$\underline{Z}_i^T \underline{Y}_k = \begin{cases} 0, & i \neq k \\ =0, & i = k \end{cases} \tag{2.19}$$

The effect of damping on the latent roots-eigenvalues will be discussed later. This will be done for a variety of fractional orders. As can be seen from (2.15 and 18), number of roots grows as $2N_x$. This will also be discussed later.

2.3
Steady state response

An alternative measure of system performance can be achieved through the use of the long time, i.e., steady state response behavior. Of particular interest is frequency amplitude and frequency phase shifting. Note, given the developments in Part I, i.e., Padovan and Sawicki (1996), the long time behavior is asymptotically the same for both the original fractional and decomposed fractional formulations of the DEQ. In this context, for the current purposes the more convenient vector representation is employed.

For the steady response, typically harmonic-periodic responses are considered. In such situations

$$S(t) \propto \cos(\omega t) \tag{2.20}$$

To establish the long time $t \gg 0$ solution to either (2.1 and 2) or its diophantine version (2.12), given that system damping washes out transient behavior, then X or $\underline{Y}$ is sought in the form

$$(X; \underline{Y}) \propto \cos(\omega t). \tag{2.21}$$

Recalling the work of Padovan and Guo (1988), it follows that

$$\lim_{t\to\infty} D_q(\cos(\omega t)) \equiv (\omega)^q \cos\ \ \omega t + \frac{\pi}{2} q \tag{2.22}$$

In this context (X, F_D) and $\underline{Y}$ can be chosen in the form:

i) General case;

$$X = \cos(\omega t) X_C + \sin(\omega t) X_S \tag{2.23}$$

$$F_D = \cos(\omega t) F_{DC} + \sin(\omega t) F_{DS} \tag{2.24}$$

ii) Diophantine;

$$\underline{Y} = \cos(\omega t)\underline{Y}_C + \sin(\omega t)\underline{Y}_S \tag{2.25}$$

Based on (2.12), the coefficients of (2.25) can be expressed as

$$\underline{Y}_\omega = [\Phi_\omega]^{-1}\underline{\ }_\omega \tag{2.26}$$

where

$$\underline{\ }^T_\omega = (\underline{\ }^T_{\omega C}, \underline{\ }^T_{\omega S}), \tag{2.27}$$

$$[\Phi_\omega] = \begin{bmatrix} (\omega)^{1/N_x}\cos\ \frac{\pi}{2N_x}\ [I] - [\Theta] & (\omega)^{(1/N)_x}\sin\ \frac{\pi}{2N_x}\ [I] \\ -(\omega)^{1/N_x}\sin\ \frac{\pi}{2N_x}\ [I] & (\omega)^{1/N_x}\cos\ \frac{\pi}{2N_x}\ [I] - [\Theta] \end{bmatrix} \tag{2.28}$$

and

$$\underline{Y}^T_\omega = \ \underline{Y}^T_C, \underline{Y}^T_S\ . \tag{2.29}$$

In terms of (2.25 and 26), the solution to (2.12) is given by the relation

$$\underline{Y} = [\cos(\omega t)[I], \sin(\omega t)[I]][\Phi_\omega]^{-1}\underline{\ }_\omega \tag{2.30}$$

To establish the phase lag in the system, we need to compare like components in $\underline{Y}_C$ and $\underline{Y}_S$ appearing in the $\underline{Y}_\omega$ vector of (2.26 and 2.29). In particular, if ϕ_i is the phase lag of the i^{th} component, then

$$\phi_i = \tan^{-1}(Y_{Ci}(\omega)/Y_{Si}(\omega)) \tag{2.31}$$

The frequency dependency can be obtained by sweeping through ω. The associated amplitude A_i frequency response follows from the relation

$$A_i(\omega) = \sqrt{(Y_{Ci}(\omega))^2 + (Y_{Si}(\omega))^2} \tag{2.32}$$

3 Model fitting

To establish a proper model, either transient or steady state spectrum data can be employed. The choice to a great extent depends on environmental factors. For the current purposes, the steady state case will be given main consideration. Based on the procedures derived, extension to transient situations represents a direct generalization of the scheme derived. Overall, the fitting process involves several main steps, namely:

1) Defining the proper empirical data set requirements;
2) Establishing the curvature properties of the empirical data;
3) Calculating diophantine approximations for the fractional power sets;
4) Developing remezed least square polynomial fit: *KV* model;
5) Developing remezed least square rational polynomial fit: *MKV* model;

This will be described in the following sections.

3.1 Empirical data

For the steady state response, generally, empirical data involves force/amplitude vs. frequency spectrum plots. Contingent on the nature of system structure, the force spectrum may involve either the net system force or alternatively the hysteretic force F_D. For simplicity, here we assume that the exciting field is harmonic. By exciting the system through a harmonic frequency sweep, $F_D(\omega)$ and $X(\omega)$ can be obtained in tabular form, i.e.,

$$\omega_i;\ F_D(\omega_i);\ X(\omega_i);\ i \in [1, N_s]$$

such, that here N_s is the number of sampling points. The spacing associated with $\omega_i;\ i \in [1, N_s]$ is dependent on the sampling rate of the experimental data.

3.2 Curvature properties of hysteretic/amplitude frequency responses

To establish the requisite basis set of fitting functions, the curvature bounds of the $F_D(\omega)$ and $X(\omega)$ spaces need to be defined. Since we are dealing with linear operators, the parametric relationship between the $F_D(\omega)$ and $X(\omega)$ takes the symbolic form

$$\frac{F_D(\omega)}{X(\omega)} = P(\omega) \tag{3.1}$$

where $P(\omega)$ is some fractional polynomial fucntion in ω. For *KV* materials, the $P(\omega)$ consists solely of a numerator polynomial, while for *MKV* media, it is a rational form. This will be seen momentarily.

To determine the form of $P(\omega)$ for *KV* media, we must consider (2.2). Under steady response conditions

$$F_D = F_{DC}\cos(\omega t) + F_{DS}\sin(\omega t) \tag{3.2}$$

$$X = X_C\cos(\omega t) + X_S\sin(\omega t) \tag{3.3}$$

Based on (3.2 and 3), the *KV* truncated version of (2.2) yields the expression

$$\underline{F}_D(\omega) = [P_N(\omega)]\underline{X}(\omega) \tag{3.4}$$

where

$$\underline{F}_D(\omega) = \begin{pmatrix} F_{DC}(\omega) \\ F_{DC}(\omega) \end{pmatrix};\ \underline{X}(\omega) = \begin{pmatrix} X_C(\omega) \\ X_S(\omega) \end{pmatrix} \tag{3.5}$$

and

$$[P_N(\omega)] = \sum_{\ell=1}^{N_x} {}_{x\ell}(\omega)^{b_\ell}[\Phi(b_\ell)] \tag{3.6}$$

such, that

$$[\Phi(b_\ell)] = \begin{bmatrix} \cos\ \frac{\pi}{2}b_\ell & \sin\ \frac{\pi}{2}b_\ell \\ -\sin\ \frac{\pi}{2}b_\ell & \cos\ \frac{\pi}{2}b_\ell \end{bmatrix} \tag{3.7}$$

For *MKV* media, (2.2), use of (3.2 and 3) yields

$$[P_D(\omega)]\underline{F}_D(\omega) = [P_N(\omega)]\underline{X}(\omega) \tag{3.8}$$

where here

$$[P_D(\omega)] = \sum_{\ell=0}^{N_f} {}_{f\ell}(\omega)^{b_\ell}[\Phi(b_\ell)] \tag{3.9}$$

Given that $[P_D(\omega)]$ is invertable, then we obtain the rational expression

$$\underline{F}_D(\omega) = [P_D(\omega)]^{-1}[P_N(\omega)]\underline{X}(\omega) \tag{3.10}$$

As can be seen from (3.4 and 10), in the frequency domain the *KV* and *MKV* models form matrix adaptations of numerator and rational polynomial forms, respectively. Here they are cast in origin centered format. For instance, noting (3.4 and 6), it follows that

$$\frac{\|\underline{F}_D(\omega)\|}{\|\underline{X}(\omega)\|} \propto \left\| \sum_{\ell=1}^{N_x} x_\ell(\omega)^{b\ell} \right\| \tag{3.11}$$

To define bounds on b_ℓ, applying the Euclidean norm to (3.9), we yield the inequality

$$\|\underline{F}_D(\omega)\| \le \|[P_N(\omega)]\|\|\underline{X}(\omega)\| \tag{3.12}$$

In view of the form of $[P_N(\omega)]$, (3.6), we have that

$$\|[P_N(\omega)]\| \le \sum_{\ell=1}^{N_x} x_\ell(\omega)^{b_\ell}\|[\Phi(b_\ell)]\| \tag{3.13}$$

where

$$1 \le \|[\Phi(b_\ell)]\| \le 4. \tag{3.14}$$

Since

$$\sum_{\ell=1}^{N_x} x_\ell(\omega)^{b_\ell} \le \max(\ _x)N_x(\omega)^{\max(b_\ell)}, \tag{3.15}$$

based on (3.13–15), (3.12) reduces to

$$\frac{\|\underline{F}_D(\omega)\|}{4N_x \max(\ _x)\|\underline{X}(\omega)\|} \le (\omega)^{\max(b_\ell)} \tag{3.16}$$

In such situations, $\underline{b} > 0$ for all k pairs. This implies that only derivative-type operators are employed in the simulation. Given, that a non-monotone functional space is involved, then two inequality types are possible, either $F_D(\omega_k) > F_D(\omega_{k+1})$, or the reverse. For such situations, successive sample point pairs yield $b_k > 0$, or $b_k < 0$. Here, the implication is that the simulation requires a range of differintegro operators. This follows from the Laurent-like form of $[P_N(\omega)]$ which leads to integral and differential operators.

For the full *MKV* model, bounds must be established from (3.8). Since such simulations yield a rational formulation, (3.10), any Laurent type terms can be cancelled out. In this context the lower bound estimates for the $\underline{a}$ and $\underline{b}$ powers can be set to zero. To set bounds on a_ℓ, we take the norm of (3.8) with $\|[P_N(\omega)]\|$ and $\|[P_D(\omega)]\|$ respectively set to their lower and upper bounds. Specifically

$$\begin{aligned} &4N_x \max(\ _f)(\omega_k)^{\max(a_\ell)}\|\underline{F}_D(\omega_k)\| \\ &\ge N_x \min(\ _x)(\omega_k)^{\min(b_\ell)}\|\underline{X}(\omega_k)\| \end{aligned} \tag{3.20}$$

Since $\min(b_\ell)$ is set to zero, (3.20) reduces to the form

$$(\omega)^{\max(a_\ell)} \ge \frac{\min(\ _x)\|\underline{X}(\omega_k)\|}{4\max(\ _f)\|\underline{F}_D(\omega_k)\|} \tag{3.21}$$

Ratioing (3.21) for subsequent ω_k pairs and taking the base 10 log, yields

$$\max(a_\ell) = \frac{\log_{10}(\|\underline{F}_D(\omega_{k+1})\|) - \log_{10}(\|\underline{F}_D(\omega_k)\|) + \log_{10}(\|\underline{X}(\omega_k)\|) - \log_{10}(\|\underline{X}(\omega_{k+1})\|)}{\log_{10}(\omega_k) - \log_{10}(\omega_{k+1})} \tag{3.22}$$

While (3.16) can be directly employed to evaluate $\max(b_\ell)$, an estimate of $\max(\ _x)$ is required. This can be bypassed by evaluating (3.16) at two subsequent ω sample points, e.g., ω_k and ω_{k+1}. Ratioing the results, we obtain the expression

$$\frac{\|\underline{F}_D(\omega_k)\|\ \|\underline{X}(\omega_{k+1})\|}{\|\underline{F}_D(\omega_{k+1})\|\ \|\underline{X}(\omega_k)\|} \sim \left(\frac{\omega_k}{\omega_{k+1}}\right)^{\max(b_k)} \tag{3.17}$$

Taking the base 10 log of (3.17), the following estimate for $\max(b_k)$ is generated, i.e.,

$$\max(b_k) = \frac{\log_{10}(\|\underline{F}_D(\omega_k)\|) - \log_{10}(\|\underline{F}_D(\omega_{k+1})\|) + \log_{10}(\|\underline{X}(\omega_{k+1})\|) - \log_{10}(\|\underline{X}(\omega_k)\|)}{\log_{10}(\omega_k) - \log_{10}(\omega_{k+1})} \tag{3.18}$$

By evaluating (3.18) over all the successive sample point pairs, the bounding value for b_ℓ can be established. Choosing the largest value, the maximum upper bound can be determined. Noting the form of the preceding expressions, a greatest lower bound can also be estimated from (3.18) by choosing the smallest value of b_ℓ from successive sample point pairs. Note, for a monotone functional space, it follows that

$$F_D(\omega_k) < F_D(\omega_{k+1}) \quad \text{for } \forall k \tag{3.19}$$

Next, to obtain $\max(b_\ell)$, the form of (3.8) is taken such that now $\|[P_N(\omega)]\|$ and $\|[P_D(\omega)]\|$ are respectively set to their upper and lower bounds. This process yields the inequality

$$\begin{aligned} &N_x \min(\ _f)(\omega_k)^{\min(a_\ell)}\|\underline{F}_D(\omega_k)\| \\ &\ge 4N_x \max(\ _x)(\omega_k)^{\max(b_\ell)}\|\underline{X}(\omega_k)\| \end{aligned} \tag{3.23}$$

Again, since $\min(a_\ell)$ is set to zero, (3.23) reduces to the expression

$$(\omega_k)^{\max(b_\ell)} \ge \frac{\min(\ _f)\|\underline{F}_D(\omega_k)\|}{\max(\ _x)\|\underline{X}(\omega_k)\|} \tag{3.24}$$

When (3.24) is ratioed for subsequent ω_k sample point pairs, the expression (3.18) is obtained again.

Together, (3.18) and (3.22) set the delimiting bounds on the denominator and numerator polynomial functions defining the rational type *MKV* simulation given by (3.10). Note, for this type simulation the denominator controls the negative slope terms. In this context, it acts like the Laurent terms of the *KV* scheme. It has the additional feature that if

selected with powers greater than the numerator, then the large ω values asymptotics are always bounded.

Note, the terms $\max(a)$, $\max(b)$, $\min(a)$, and $\min(b)$ set the bounding constraints on the $\underline{a}$ and $\underline{b}$ power sets. From the integerized point of view we obtain:

i) upper bound (for both *KV* and *MKV*);

$$(I^{fU}; I^{xU}) \geq \max(a_\ell, b_\ell) \tag{3.25}$$

ii) lower bound (*KV*);

$$I^{xL} \quad \min(b_\ell) \tag{3.26}$$

iii) lower bound (*MKV*);

$$(I^{fL}; I^{xL}) \leq (0; 0) \tag{3.27}$$

Conditions (3.25–27) can be employed to establish the diophantine approximation to the power sets. This yields the a_ℓ and b_ℓ family of rational integer defined fractional power sets.

3.3 KV fit

To establish the *KV* fit, (3.4) must be made to satisfy $\underline{F}_D(\omega_k)$ and $\underline{X}(\omega_k)$ for all ω_k arising from the experimental sample point data set. Given that such sets are typically quite large, the best fit may be affected by say a least scheme. To provide for the most complete fractional basis space, N_x of the b_ℓ set is raised to the requisite level. In this context, $[P_N(\omega)]$ of (3.4) takes the diophatinized form

$$[P_n(\omega_k)] = \sum_{\ell=1}^{N_x} {}_{x\ell}(\omega)^{b_\ell}[\Phi(b_\ell)] \tag{3.28}$$

Since we seek the set of fitting coefficients $\underline{}_x$, (3.4) must be altered. As $\underline{F}_D$ and $\underline{X}$ are the given, rearranging coefficients we yield the algorithm

$$\underline{F}_D(\omega) = [\Psi_N(\omega)]\underline{}_x \tag{3.29}$$

such, that

$$[\Psi_N(\omega)] = \ \ldots, (\omega)^{b_\ell}[\Phi(b_\ell)]\underline{X}(\omega), \ldots \tag{3.30}$$

wherein $\ell \in [1, N_x]$ and $[\Psi_N(\omega)]$ is a $[2, N_x]$ coefficient matrix. When the number of sampling points is greater than N_x, (3.29) is in a modest state of error for any given sampling point ω_k. Hence,

$$\underline{\xi}_k = \underline{F}_D(\omega_k) - [\Psi_N(\omega_k)]\underline{}_x \tag{3.31}$$

where $\underline{\xi}_k$ is the k^{th} error vector. Forming the least square net error term, we yield the relation

$$\xi = \sum_k \underline{\xi}'_k \ \underline{\xi}_k \tag{3.32}$$

Based on the form of (3.31), it follows that ξ is a function of the vector of fitting coefficients $\underline{}_x$.
To minimize ξ, we seek $\underline{}_x$ which satisfy the condition

$$d\xi = 0 = \quad 2d\underline{\xi}'_k \ \underline{\xi}_k \tag{3.33}$$

Recalling the form of $\underline{\xi}_k$, i.e., (3.31), it follows that (3.33) yields the optimality condition

$$\underline{}_x \equiv [Z_N]^{-1}\underline{\xi}_N \tag{3.34}$$

where

$$\underline{\xi}_N = \sum_k [\Psi_N(\omega_k)]^T \underline{F}_{Dk} \tag{3.35}$$

$$[Z_N] = \sum_k [\Psi_N(\omega_k)]^T [\Psi_N(\omega_k)] \tag{3.36}$$

with

$$[\Psi_N(\omega_k)] \equiv \ \ldots, (\omega_k)^{b_\ell}[\Phi(b_\ell)]\underline{X}(\omega_k), \ldots \tag{3.37}$$

In setting up (3.29), the first iteration involves the use of the original sample distribution ω_k. While the foregoing least square scheme reduces the net error, it is possible that the local, i.e., pointwise errors may be very significant. To provide the fit with a uniform, i.e., Chebyshev type error distribution, the Remez (1934) scheme can be employed to redistribute the sample point space. Specifically, by focusing in on the local error distribution, the Remez (1934) scheme enables a redistribution of ω_k points so as to yield a more or less uniform optimal error. This requires the definition of the local error vector $\underline{\xi}_L$. In the context of (3.31), $\underline{\xi}_L$ can be written in the form

$$\underline{\xi}_L = \underline{F}_D(\omega_L) - [\Psi_N(\omega_L)]\underline{}_x \tag{3.38}$$

such that, ω_L is the local frequency value wherein $\underline{F}_D(\omega_L)$ and $\underline{X}(\omega_L)$ are estimated by interpolations formed from higher order spline fits, see Ahlberg et al. (1967). To obtain a scalar version of the error, an inner product can be taken, namely:

$$\xi = \sum_L \underline{\xi}'_L \ \underline{\xi}_L \tag{3.39}$$

Once the ξ_L vs. ω_L distribution is determined, the sample points can be redistributed to zones of larger ξ_L. This can be achieved by essentially direct proportionality. In particular, once a given number of sample points are equally spaced, the remainder are redistributed in direct proportion to the local error density. Such a redistribution can be undertaken recursively until the requisite convergence criteria are met. The recursion process involves cyclic applications of the least square and Remez steps. This results in accuracy levels which provide both, minimal ξ values, as well as a more or less uniform error over the sample space range.

3.4 MKV fit

In the context of the *KV* fit, the *MKV* simulation can be established through the use of (3.8). Based on the diophantine form of $[P(\omega)]$, we assume the coefficient of the zeroth order derivative of F_D to be monic. In this context, Eq. (3.9) can be recast as follows

$$[P_D(\omega)] = [I] + \sum_{\ell=1}^{Nf} {}_{f\ell}(\omega)^{a_\ell}[\Phi(a_\ell)] \tag{3.40}$$

where $[I]$ is an identity matrix. For convenience, since we seek $\underline{}_f$, the second term appearing in (3.40) can be recast as

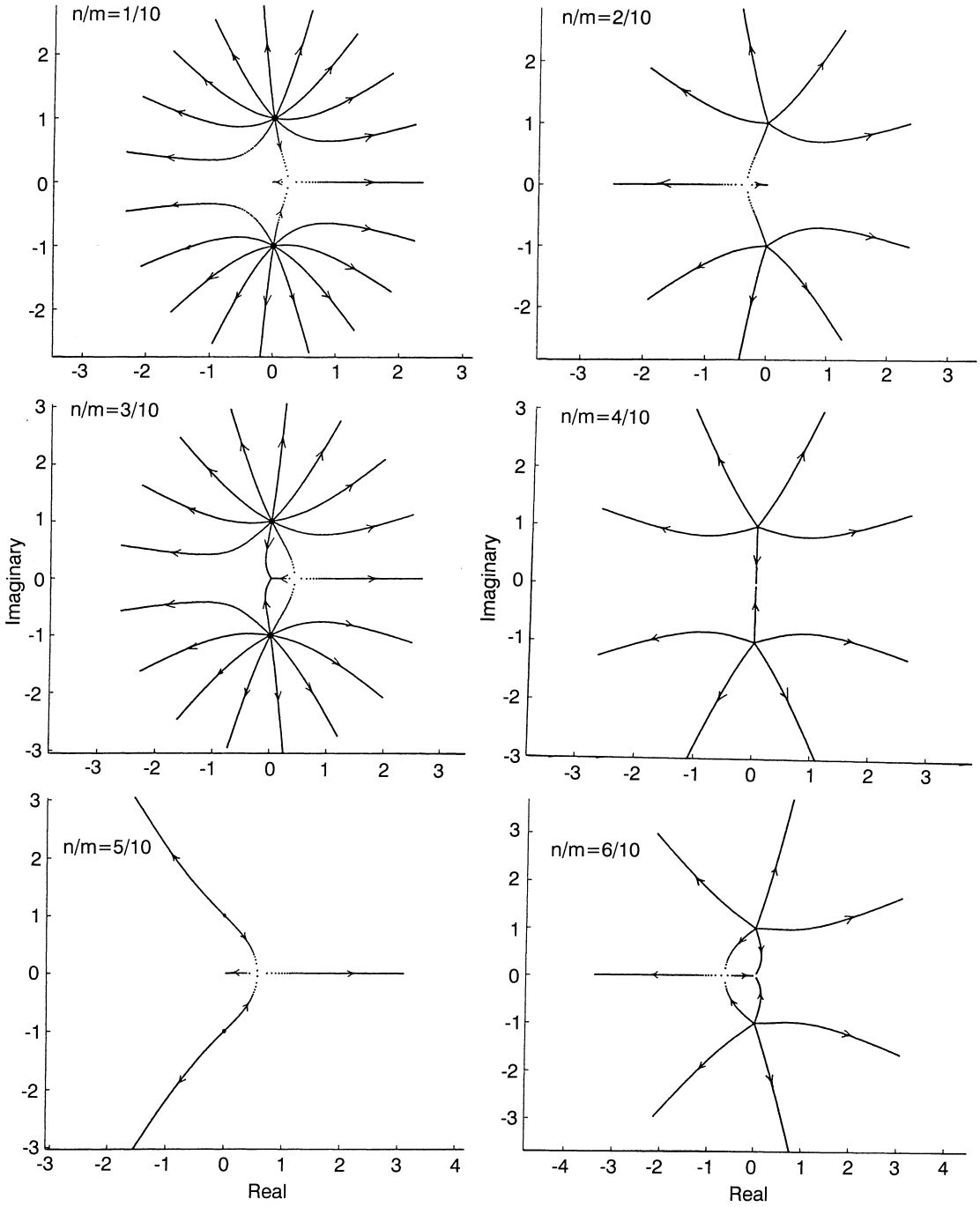

Fig. 1. Root locus: $(n/m) \in [1/10, 6/10]$; variations

$$\sum_{\ell=1}^{N_f} {}_{f\ell}(\omega)^{a_\ell}[\Phi(a_\ell)]\underline{F}_D(\omega) \equiv [\Psi(\omega)]_{\_f} \tag{3.41}$$

such, that

$$[\Psi_D(\omega)] = [\ldots, (\omega)^{a_\ell}[\Phi(a_\ell)]\underline{F}_D(\omega), \ldots] \tag{3.42}$$

Based on (3.40 and 41), (3.8) reduces to the more convenient form

$$\underline{F}_D(\omega) + [\Psi_D(\omega)]\underline{F}_D(\omega) = [\Psi_N(\omega)]\underline{X}(\omega) \tag{3.43}$$

The local error vector associated with (3.43) takes the form

$$_{\_k} = \underline{F}_D(\omega_k) + [\Psi_{DN}(\omega_k)]_{\_fx} \tag{3.44}$$

where

$$_{\_fx} = \begin{matrix} {}_{\_f} \\ {}_{\_x} \end{matrix} \tag{3.45}$$

and

$$[\Psi_{DN}(\omega)] = [-[\Psi_D(\omega)], [\Psi_N(\omega)]] \tag{3.46}$$

As before, forming the least square error expression, we yield (3.39). Seeking the extremum criterion, we obtain the identity

$$_{\_fx} = [Z_{DN}]^{-1}{}_{\_DN} \tag{3.47}$$

such that

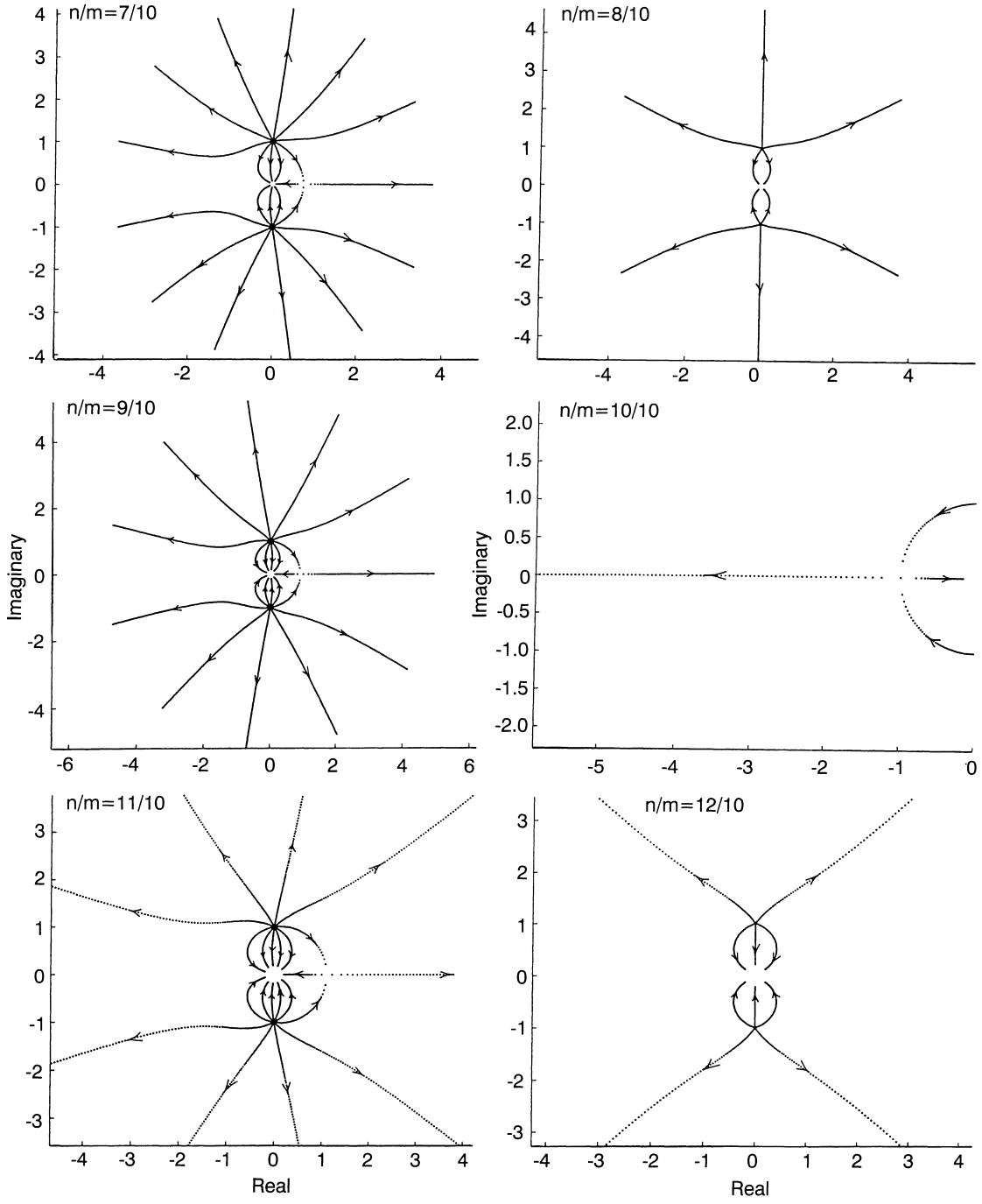

Fig. 2. Root locus: $(n/m) \in [7/10, 12/10]$; variations

$$[Z_{DN}] = \sum_k [\Psi_{DN}(\omega_k)]^T [\Psi_{DN}(\omega_k)] \tag{3.48}$$

and

$$\underline{\ }_{DN} = \sum_k [\Psi_{DN}(\omega_k)] \underline{F}_D(\omega_k) \tag{3.49}$$

The remezed least square cycle of iterative improvements follows as before.

4
Model correlation

To illustrate the fractional modeling scheme, several issues will be addressed. These include:

i) Eigenvalue properties of fractional formulations of varying orders;
ii) Phase lag behavior;
iii) Frequency amplitude behavior, and;
iv) Correlation performance for various frequency dependent problems.

This will be described in the following subsections.

4.1
Eigen properties

For the current purposes, we shall consider the eigen properties of fractional simulations of varying orders and

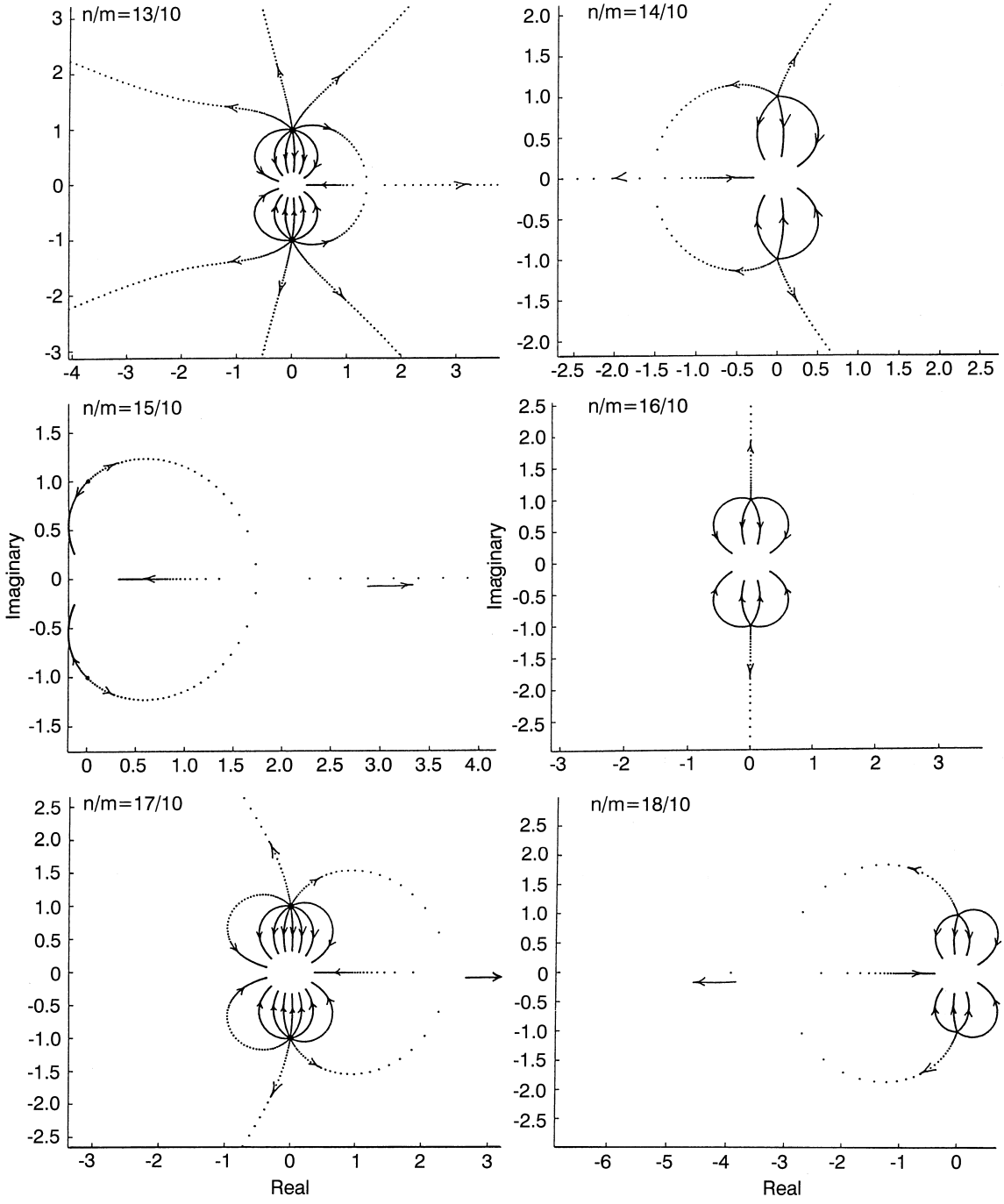

Fig. 3. Root locus: $(n/m) \in [12/10, 18/10]$; variations

overall form. To determine the main features, the diophantine representation will be employed. Two main operator expressions will be considered, i.e.,

1) a single term hysteretic representation, and;
2) a multiple term simulation.

For instance, the single term model can be written as follows

$$D_2(x) + \quad D_{n/m}(x) + \omega^2 x = 0, \quad n < 2m \tag{4.1}$$

Cast in vector form we yield the expression

$$D_{\frac{1}{m}}(\underline{Y}) = [\Theta_{nm}]\underline{Y} \tag{4.2}$$

wherein $[\Theta]$ is $(2m \times 2m)$, and

$$\underline{Y}^T = (Y_0, Y_1, Y_2, \ldots, Y_{2m-1}) \tag{4.3}$$

$$[\Theta_{nm}] = \begin{vmatrix} 0 & 1 & 0 & \cdots & 0 & \cdots & 0 \\ 0 & 0 & 1 & & 0 & & 0 \\ \vdots & & & \ddots & \vdots & & \vdots \\ 0 & 0 & 0 & \cdots & 1 & & 0 \\ \vdots & & & & & \ddots & \vdots \\ 0 & 0 & 0 & & 0 & & 1 \\ -\omega^2 & 0 & 0 & \cdots & - & \cdots & 0 \end{vmatrix} \tag{4.4}$$

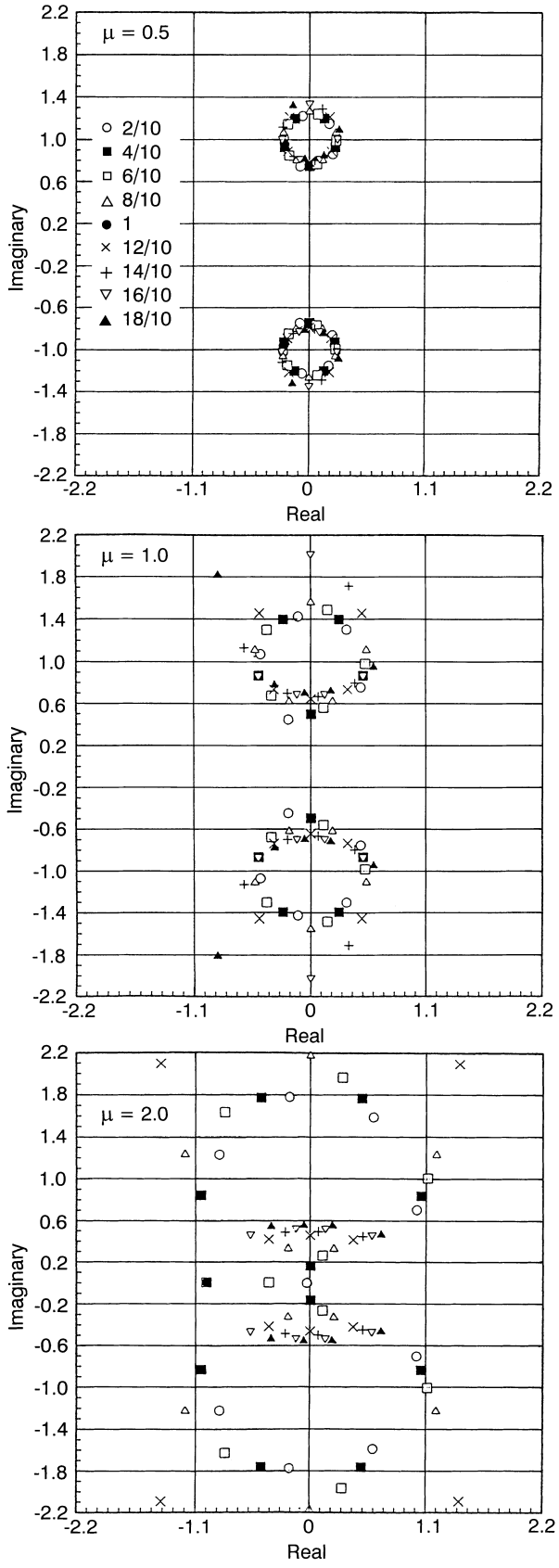

Fig. 4. Root locus for n/m variations for fixed value

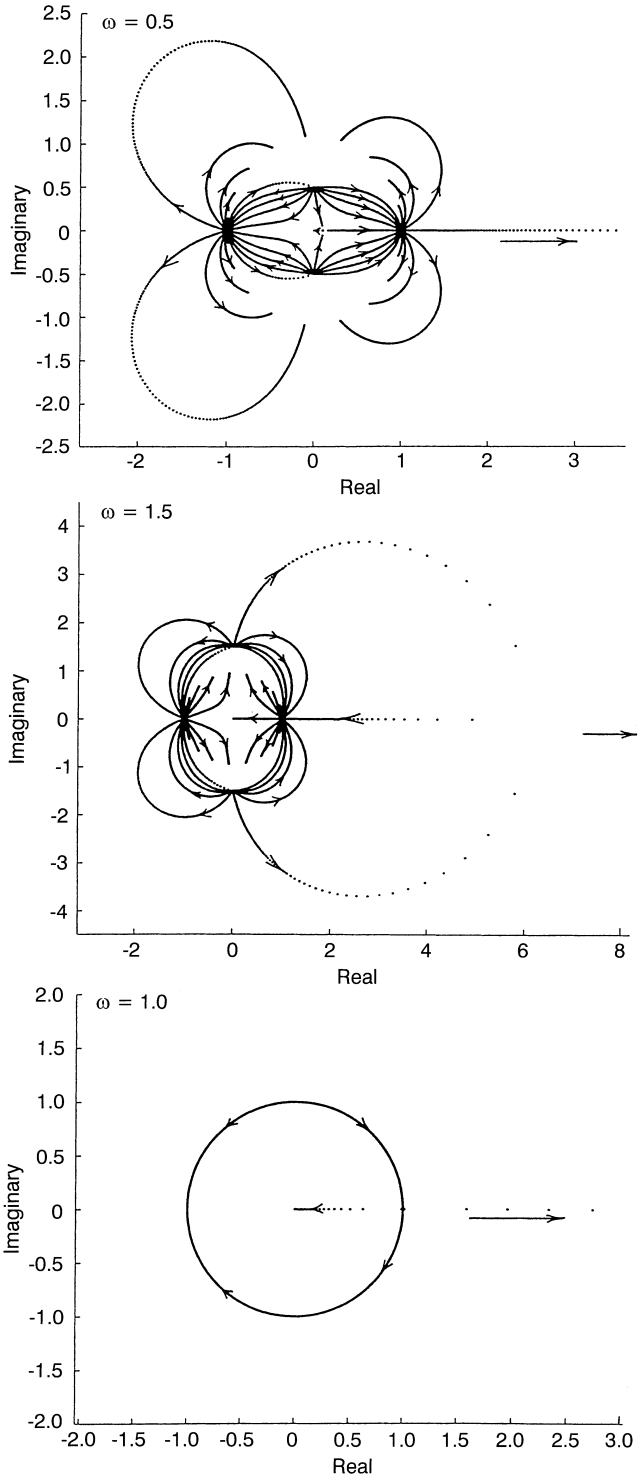

Fig. 5. Root locus variations on for multiple term simulation: $_n =$ for $n; m = 10, n \in [1, 19]$

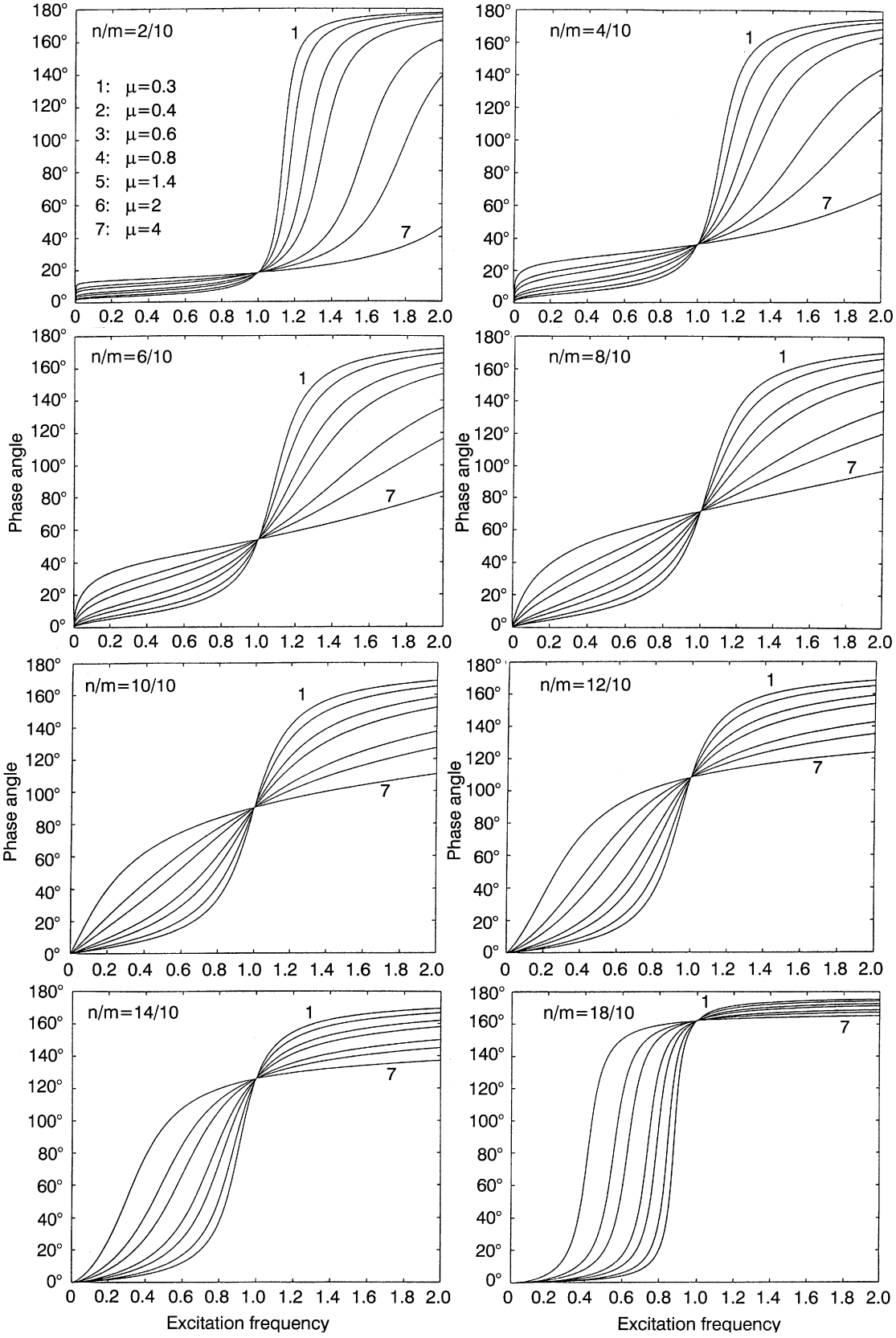

Fig. 6. Phase lag for single term model for μ variations and $n/m \in [0.2, 1.8]$

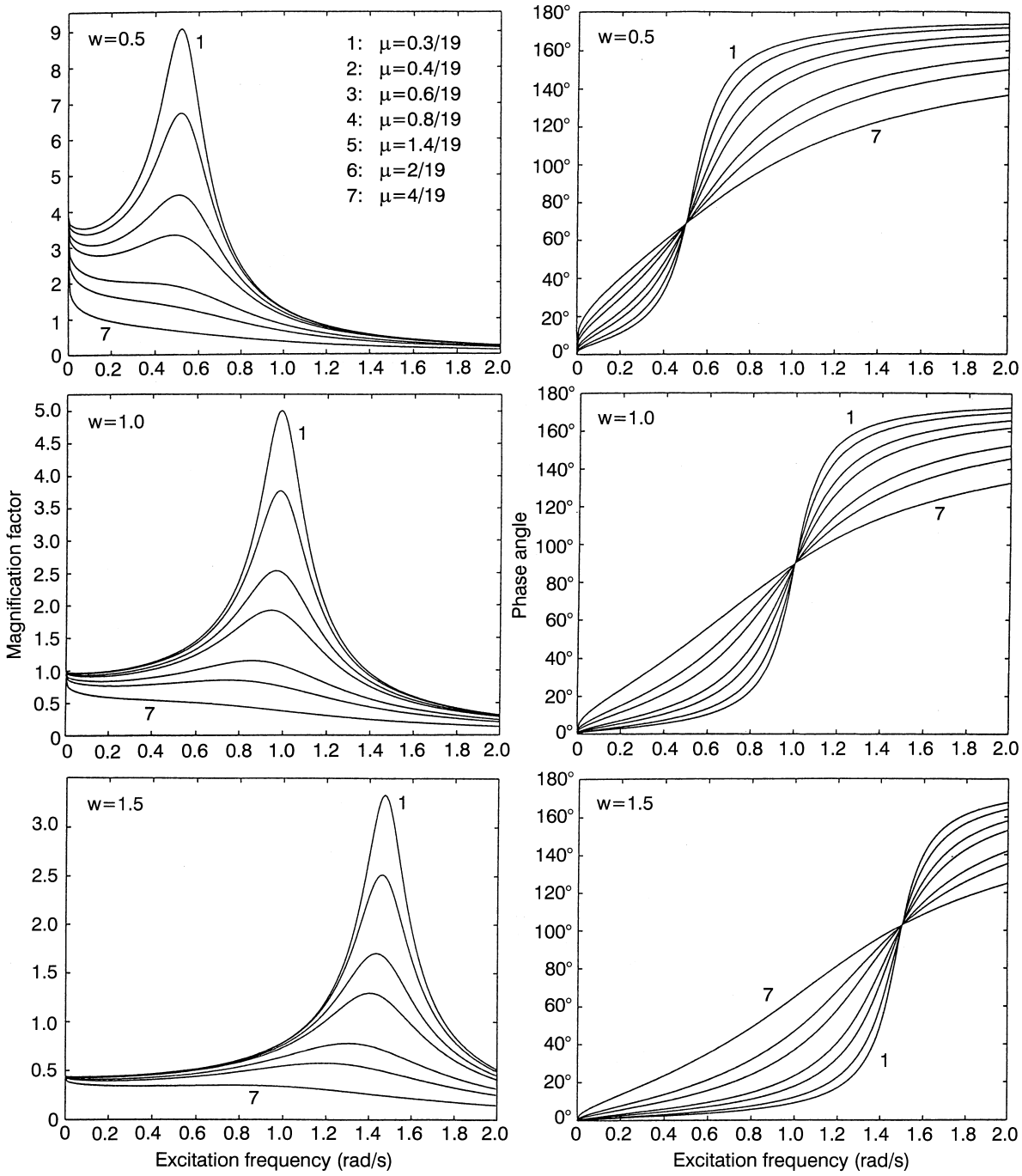

Fig. 7. Phase lag (right column) and amplitude frequency response (left column) for multiple term model variations and $n/m \in [0.2, 1.8]$

Equation (4.2) possesses the following linear eigen problem

$$(s)^{1/m}\underline{y} - [\Theta]\underline{y} = \underline{0} \tag{4.5}$$

In the case of the multiple term simulation, the equation of motion has the form

$$D_2(x) + \sum_{n=1}^{2m-1} {}_nD_{n/m}(x) + \omega^2 x = 0 \tag{4.6}$$

Cast as a vector, relation (4.6) yields the following expression for $[\Theta_{nm}]$,

$$[\Theta_{nm}] = \begin{vmatrix} 0 & 1 & 0 & \cdots & 0 \\ 0 & 0 & 1 & \cdots & 0 \\ \vdots & & & \ddots & \vdots \\ 0 & 0 & 0 & \cdots & 1 \\ -\omega^2 & -{}_1 & -{}_2 & \cdots & -{}_{2m-1} \end{vmatrix} \tag{4.7}$$

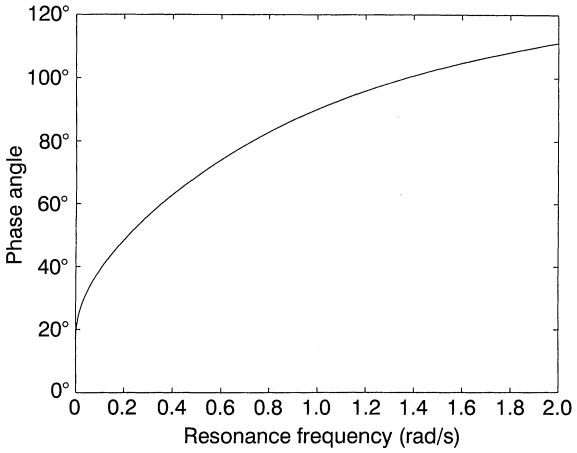

Fig. 8. Phase angle versus resonance frequency for multiple term simulation: $n/m \in [0.1, 1.9]$

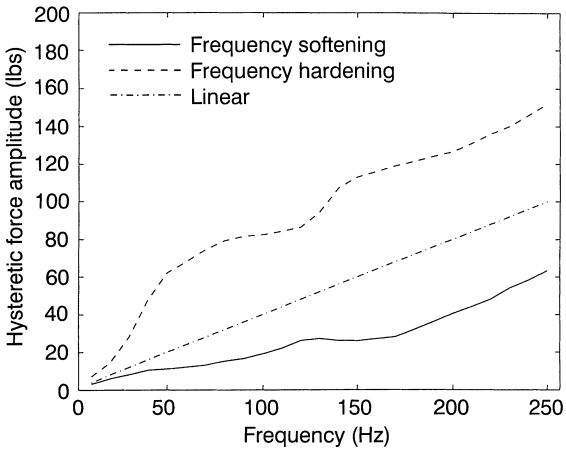

Fig. 10. Frequency hardening/softening/linearity of force deflection response

Figs. 1–4 illustrate the root locus for variation in n/m and . As can be seen, for $n = m$, the traditional viscous roots are obtained. Figure 5 gives the root locus for variations in for the multiple term simulation, i.e., wherein $m = 10$ and $n \in [1, 2m-1]$. Here, $= {}_n$ for all n, and the root locus is presented for three different system natural frequencies, i.e., $\omega = 0.5$, 1.0 and 1.5 rad/s.

4.2
Phase lag behavior

Recalling the steady state solution, i.e., Eq. (2.26), the phase lag is defined by the relative sizes of the components of the displacement vector $\underline{Y}$. Figure 6 illustrates the phase lag behavior for the single term simulation. In this case the phase angle at resonance frequency does not depend on the system natural frequency and is equal to $\frac{\pi}{2}\ \frac{n}{m}$. For $n/m < 1$ the resonance phase angle tends to zero, whereas for $n/m > 1$ it tends to 180°. The phase lag behavior for multiterm simulation (4.6) is shown in the right column of Fig. 7. Here, $= \frac{n}{2m-1}$ for all n, and $m = 10$. The magnitude of the frequency dependent resonance phase angle can be expressed as

$$\phi_{resonance} = \frac{\sum_i \omega^{q_i - 1} \sin(\pi q_i/2)}{\sum_i \omega^{q_i - 1} \cos(\pi q_i/2)} \tag{4.8}$$

where ω is the resonance frequency and $q_i = \frac{i}{m}$, for $i \in [1, 2m-1]$. The locus of phase lag values versus resonance frequency is illustrated in Fig. 8. For the multiple term simulation, the behavior is dependent on the mix of coefficient magnitudes. This of course is dictated by problem physics. Note, since both components of $\underline{F}_D$ and $\underline{Y}$ are fitted by the scheme developed, any form of phase lag can be handled.

4.3
Amplitude behavior

Based on Eq. (2.26), Figs. 7 (left column) and 9 illustrate the amplitude-frequency behavior for the multiple and single term models, respectively. As can be seen from Fig. 9, for $n/m < 1$, the peak amplitude may occur at frequencies greater than the natural. For $n/m \geq 1$, the peak occurs for frequencies lower than the natural. This phenomenon, caused by the stiffening (for $n/m < 1$) or softening (for $n/m \geq 1$) of the system, indicates that the fractional representation provide richer capabilities to model material response behavior over the frequency range. Note, in the multiterm fit, all such behavior is captured contingent on the empirical data defining hysteretic behavior.

4.4
Correlation studies

Under many circumstances, the hysteretic performance of a given system may either be constant, weekly, or strongly

Table 1. Force-amplitude/frequency response: hardening

Frequency	Hardening	
	Cosine	Sine
10	7.1	1.0
20	14.3	2.0
30	28.2	5.2
40	48.1	13.1
50	62.05	20.5
60	68.1	33.1
70	74.5	40.5
80	79.2	44.1
90	81.5	53.3
100	82.4	57.1
110	84.2	59.4
120	86.3	62.05
130	94.4	65.7
140	107.2	69.1
150	113.1	71.1
160	116.0	72.4
170	119.0	78.1
180	121.5	80.7
190	124.5	87.2
200	126.7	88.7
210	131.2	94.3
220	136.0	97.1
230	140.2	103.4
240	146.0	106.3
250	152.0	110.2

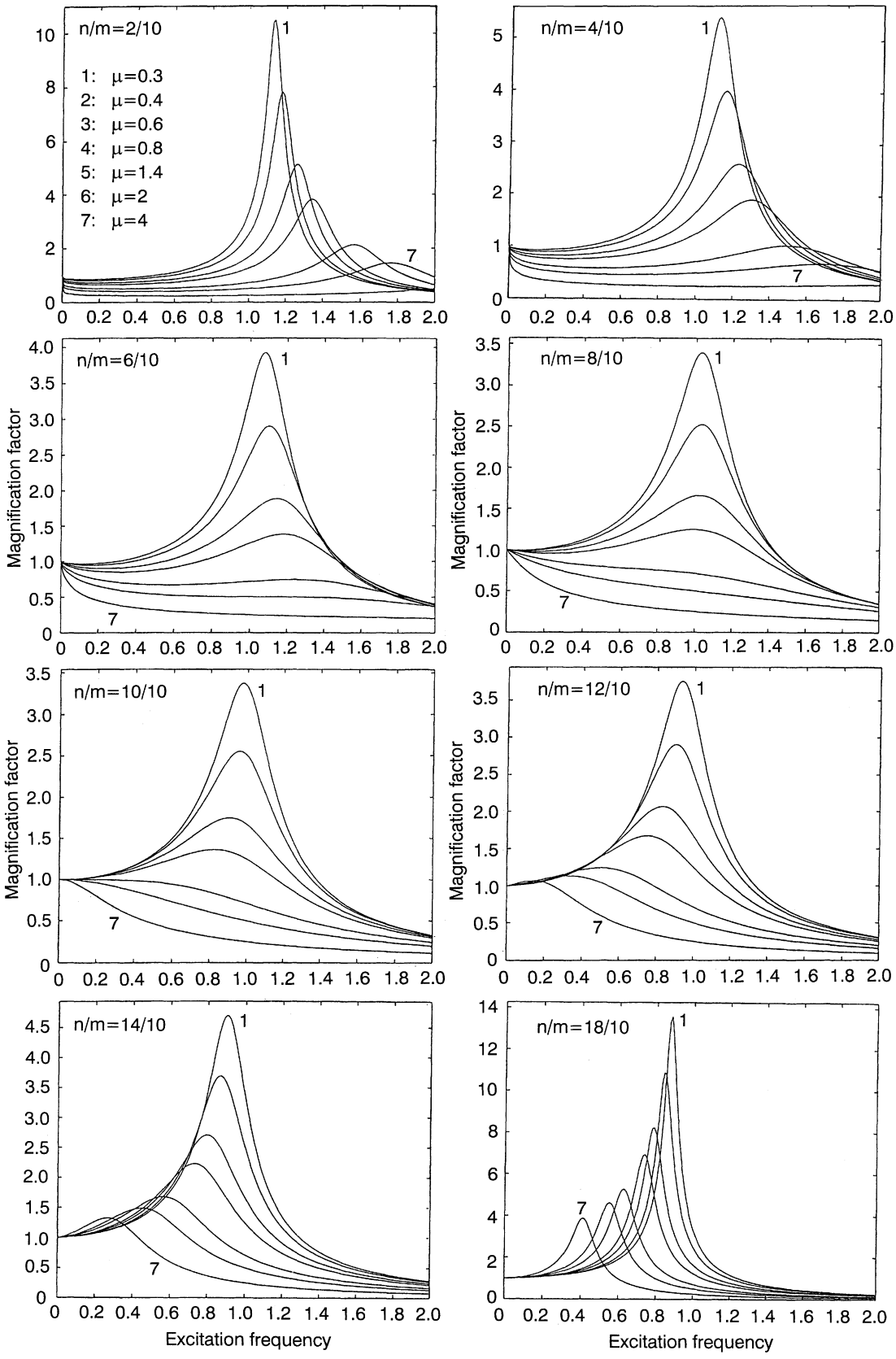

Fig. 9. Amplitude frequency response for single term model for μ variations and $n/m \in [0.2, 1.8]$

frequency dependent. Such behavior may be monotone increasing, decreasing or in general non-monotone. Typically, for higher frequencies, the behavior tends to stiffen, i.e., require more energy to yield the same amplitude as frequency increases. Figure 10 illustrates the foregoing frequency softening and hardening. Such behavior is es-

Table 2. Force-amplitude/frequency response: softening

Frequency	Softening	
	Cosine	Sine
10	3.2	1.1
20	6.01	2.2
30	8.15	3.1
40	10.5	4.2
50	11.1	5.1
60	12.07	6.2
70	13.01	5.3
80	15.2	4.2
90	16.5	4.1
100	19.1	5.1
110	22.05	7.2
120	26.01	9.4
130	27.2	8.4
140	26.05	8.2
150	26.1	8.1
160	27.2	10.5
170	28.2	11.5
180	32.1	12.5
190	36.2	15.1
200	40.5	24.0
210	44.2	28.5
220	48.2	28.0
230	54.3	31.0
240	58.2	36.1
250	63.4	38.4

sentially an outgrowth of potential frequency dependent hysteretic effects. This follows from the fact that for linear viscous damping, the force and displacement amplitudes are related by the identity

$$\underline{F}_D(\omega) \propto C\omega[I_s]\underline{X}(\omega) \tag{4.9}$$

where $[I_s]$ is a skew symmetric one matrix. Equation (4.9) illustrates the typical linear frequency dependence of such models. In view of the skew symmetry associated with (4.9), it follows that the velocity and force are essentially in what may be termed "*in hysteretic phase*". This implies that the I/O fields associated with the linear viscous type dissipative process are in phase. Such behavior is not to be confused with the traditional phasing, which involves the interaction between mass and stiffness effects causing frequency passing shifts.

For the more general *MKV* models, the relationship between $\underline{F}_D$ and $\underline{X}$ follows from (3.8). Here, the matrix

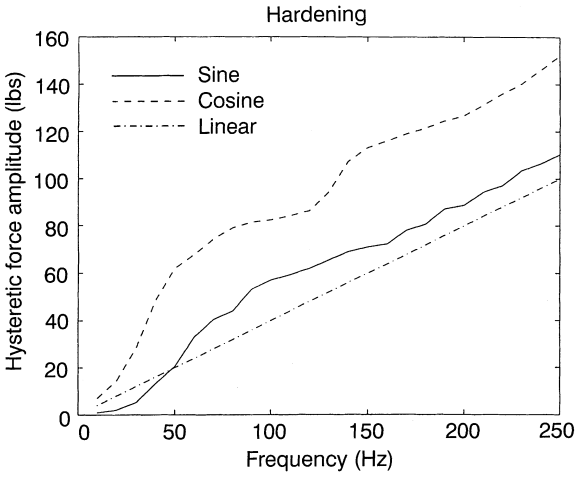

ig. 1. Hardening behavior of hysteretic forces and kinematics in frequency space

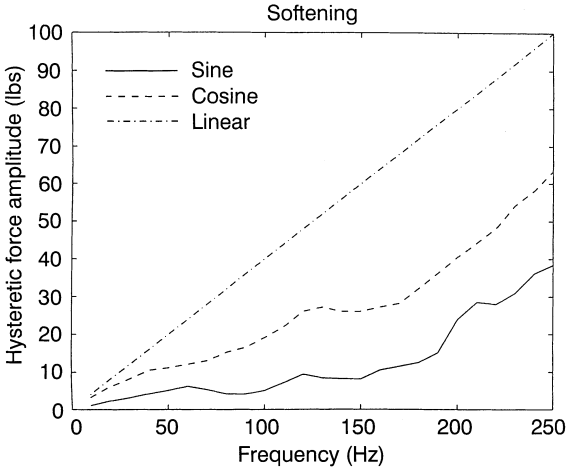

Fig. 12. Softening behavior of hysteretic forces and kinematics in frequency space

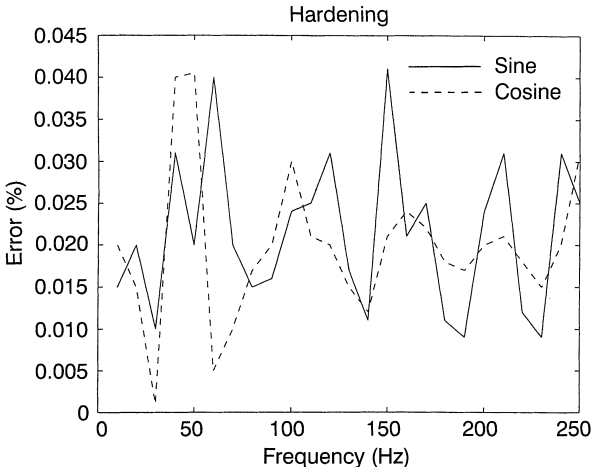

Fig. 13. Correlation of integer and fractional *KV* and *MKV* fits of Table 4.1 data: hardening model: error in fitting range

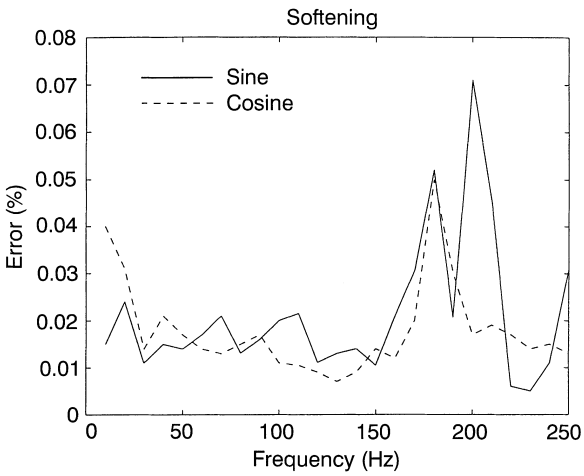

Fig. 14. Correlation of integer and fractional *KV* and *MKV* fits of Table 4.2 data: softening model: error in fitting range

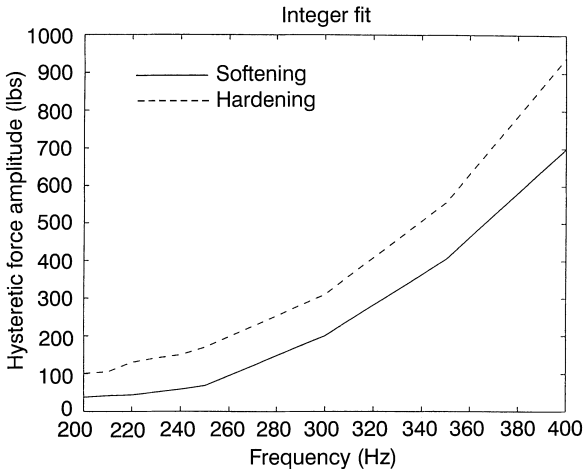

Fig. 15. Improper asymptotics *KV*; integer fit

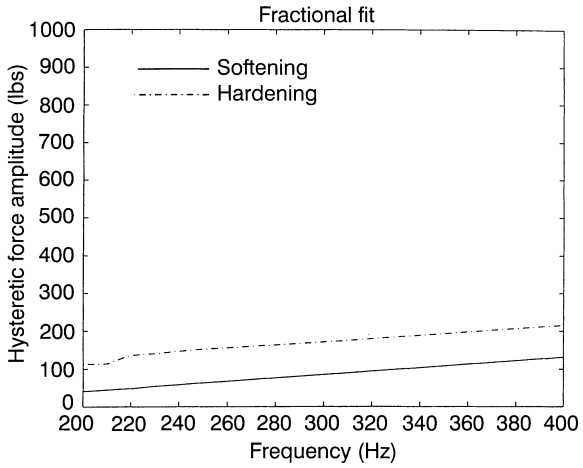

ig. 16. Proper asymptotics *KV*; fractional fit

properties of $[P_D]$ and $[P_N]$ are structured by the $[\Phi(p)]$ family, wherein $p \in (\underline{p}^x$ or $\underline{p}^f)$. In view of such characteristics, the off-diagonal components of $[P_N]$ and $[P_D]$ form their skew symmetric parts. Given that a prescribed displacement history is employed to define the various properties appearing in the *MKV* formulation, (3.10) can be used to define the force-kinematic response behavior in the frequency domain. Based on the foregoing, the matrix coefficient appearing in (3.10) has the form

$$[P_D(\omega)]^{-1}[P_N(\omega)] = \begin{matrix} \alpha\beta \\ -\beta\alpha \end{matrix} \tag{4.10}$$

For kinematic inputs phased so that $x_s \equiv 0$, the I/O relationship reduces to the frequency dependent expressions:

$$F_{DC} = \quad (\omega)X_c(\omega) \tag{4.11}$$

$$F_{DS} = -\beta(\omega)X_c(\omega) \tag{4.12}$$

Tables 1 and 2 illustrate the force-amplitude (kinematic) frequency response for hardening and softening type behavior, respectively. Figures 11 and 12 illustrate such characteristics. For demonstration purposes, Figs. 13 and 14 depict least square fitting errors for the integer and fractional representations of the examples depicted in Figs. 11 and 12 and Tables 1 and 2. In the region of fitting, it is clear that the fractional approach yields improved results for a smaller number of basis terms. This is true for both the *KV* and *MKV* representations.

In applications beyond the range of fitting, the integer fit yields completely unstable results for both the *MKV* and *KV* models. This follows from the fact that the higher order terms dominate in such upper ranges of ω, hence leading to improper asymptotics, Fig. 15. In contrast, since bounding estimates were made for the fractional representation, more controlled asymptotics can be expected, Fig. 16. An additional feature of the fractional representation follows from the close spacing powers as the basis space is enriched. Because of this, no single term can completely dominate the asymptotics. Rather, a large number of closely spaced powers contribute to the large ω response.

In the context of the foregoing results, it follows that fractional hysteretic representations have superior performance characteristics over their integer counterpart. As can been seen, in their diophantine approximated version, fractional fits have very convenient numerical characteristics. By evaluating the bounding curvature properties of the problem, the diophantine family of powers provide for:

1) very stable asymptotics;
2) essentially complete basis of fitting functions;
3) can be reduced to a state space form with associated biorthogonal properties; and
4) can handle wide range of problem curvatures.

References

1. **Ahlberg, J. H.; Nilson, E. N.; Walsh, J. L.** (1967): The Theory of Splines and their Applications. New York: Academic Press
2. **Carpenter, A. J.; Varga, R. S.** (1991): Some Numerical Results on Best Uniform Polynomial Approximation of x on [0,1] In: Gonchar, A. A., Saff, E. B. (ed): Methods of Approximation Theory in Complex Analysis and Mathematical Physics, 192–222. New York: Springer
3. **Hamming, R. W.** (1962): Numerical Methods for Scientists and Engineers. New York: McGraw-Hill
4. **Padovan, J.; Guo, Y. H.** (1988): General Response of Viscoelastic System Modeled by Fractional Operators. Journal of Franklin Institute 325, 247–275
5. **Padovan, J.; Sawicki, J. T.** (1997): Diophantine Type Fractional Derivative Representation of Structural Hysteresis, Part I: Formulation. Computational Mechanics 19, 335–340
6. **Remez, E. Y.** (1934): Sur le Calcul Effectiv des Polynomes d'Approximation de Tchebichef, CR Acad. Sci, Paris 199, 337–340,
7. **Schmidt, W. M.** (1980): Diophantine Approximation. New York: Springer

Post-print standardized by MSL Academic Endeavors, the imprint of the Michael Schwartz Library at Cleveland State University, 2014